Master's Dissertation of Department of Medicine

Ideal Size Range for Embolic Agents in Interventional Oncology Experiments involving Rat models of Hepatocellular Carcinoma

쥐 간세포암 모델을 이용한 중재적 종양학 실험에서 색전물질의 이상적인 크기

August 2022

Graduate School of Medicine
Seoul National University
Department of Radiology Major

Seong Ho Kim

Ideal Size Range for Embolic Agents in Interventional Oncology Experiments involving Rat Models of Hepatocellular Carcinoma

지도교수 정진욱

이 논문을 의학석사 학위논문으로 제출함

2022년 4월

서울대학교 대학원
의학과 영상의학 전공

김 성 호

김성호의 의학석사 학위논문을 인준함

2022년 7월

위 원 장 _____ (인)
부 위 원 장 _____ (인)
위 원 _____ (인)

Abstract

Objective

To optimize future translational research, the present study aimed to determine the ideal range of sizes for embolic agents in interventional oncology experiments utilizing rat models of hepatocellular carcinoma.

Materials and Methods

Fifty-four male Sprague–Dawley rats were randomly divided into two groups to evaluate the distribution of microparticles and tumor response rates. After implanting hepatoma cells into the rodent liver, fluorescent microparticles of diverse size ranges were administered via the hepatic artery. In the first group, the distribution of microparticles was evaluated in hepatoma-free rats, and tumor necrosis rates following administration of the pre-determined amounts of microparticles were measured in tumor-bearing rats. Afterwards, the three microparticle sizes associated with the best tumor response rates were chosen for analysis of tumor necrosis rates following complete hepatic artery embolization in the second group.

Results

The tendency for microparticles to distribute in non-target organs increased as microparticle size decreased below 15 μm. Tumor necrosis rates tended to be higher in rats treated with 15–19-μm microparticles than

in those treated with 18–24.9-μm or 25–35-μm microparticles. The in-group deviation of tumor necrosis rates was highest for microparticle sizes of 18–24.9 μm and 25–35 μm, which implies proximal embolization of the hepatic artery for larger microparticle sizes. However, there was no statistically significance among the three groups (p = .095).

Conclusion

These results suggest that embolic agents ranging in size from 15–19 μm should be considered as the first option for achieving tumoricidal effects via transarterial treatments in rat models of HCC.

Keyword : Transarterial embolization, Embolic agent, Microparticle, Hepatocellular Carcinoma, Rat, Animal experiment

Student Number : 2014-25048

요약 (국문초록)

연구 목적

본 연구는 쥐의 간세포암 모델을 이용하여 색전물질의 이상적인 크기를 결정하는 것을 목적으로 하였다.

연구 방법

54 마리의 수컷 Sprague-Dawley 쥐를 무작위로 2 개의 군으로 나누어 한 군은 종양 및 장기 별 미세입자의 분포를 평가하고, 한 군은 종양 반응을 평가하였다. 첫번째 군의 일부 쥐와 두번째 군의 모든 쥐에서 간세포암 세포를 쥐의 간에 이식하였고, 이후 다양한 크기의 형광입자를 모든 쥐의 간동맥을 통하여 주입하였다. 첫번째 군은 간세포암이 없는 쥐와 간세포암이 있는 쥐로 나뉘는데, 간세포암이 없는 쥐에서는 각 장기별 미세입자의 분포를 분석하였고, 간세포암이 있는 쥐에서는 종양 및 각 장기별 미세입자의 분포 뿐만이 아니라 종양 괴사율을 계산하였다. 두번째 군에서는 앞에서 계산한 종양 괴사율이

높은 3 가지 크기의 미세입자를 골라 쥐의 간동맥을 완전히 막은 후 이에 따른 종양 괴사율을 분석하였다.

연구 결과

미세입자의 크기가 작을수록 비표적 장기로 미세입자가 분포되는 경향이 있었다. Nile Red 입자의 크기가 15 μm 이상이었을 때는, 한 마리의 쥐만 제외하고 나머지 쥐에서 3 개 이하의 미세입자가 폐에서 검출되었다. 종양 괴사율은 15–19 μm 크기의 미세입자를 사용한 색전술군이 18–24.9 μm 와 25–35 μm 입자를 사용한 색전술군보다 더 높은 종양 괴사율을 보였다. 한편 18–24.9 μm 와 25–35 μm 입자를 사용한 색전술군은 종양 괴사율의 군내 편차도 컸는데, 이는 너무 큰 입자가 원위부 색전을 유발하였기 때문으로 추측된다. 그러나 세 그룹간 종양 괴사율의 차이가 통계적으로 유의한 수준에는 도달하지 않았다 (p = .095).

결론

쥐의 간세포암 모델을 이용한 경동맥 색전술 실험에서 충분한 색전효과를 얻기 위해서는 약 15 – 19 μm 크기의 색전 물질을 사용하는 것이 권장된다.

주요어

경동맥색전술, 색전 물질, 미세입자, 간세포암, 쥐, 동물 실험

학번 : 2014-25048

List of Tables and Figures

Table of Contents

Introduction

Animal models, particularly rat models of hepatocellular carcinoma (HCC), are widely utilized in interventional oncology research [1-3]. Rat models have several advantages over larger animal models (e.g., easier to breed and handle), and numerous innovative rat experiments have been described in the literature [4-6]. In addition, percutaneous catheterization of the rat hepatic artery allows the experimenter to simulate intra-arterial infusion of chemoembolic agents in humans [7-13]. Accordingly, knowledge regarding HCC has advanced greatly over the last decade due to research involving rat models.

McA-RH7777 cells in Buffalo rats, N1-S1 cells in Sprague–Dawley rats, and the fusion of the two models (McA-RH7777 cells in Sprague-Dawley rats) are commonly utilized to investigate transarterial treatments in rat models of HCC [14, 15]. Some groups have also proposed 13762-MAT-B-III cells in F344 rats as a model of hypervascular liver metastasis [16, 17]. As each model has its own strengths and weaknesses, the ideal rat model for interventional oncology experiments is selected based on the purpose of the investigation.

However, the ideal size of embolic agents in rat hepatoma models remains to be elucidated. Prior studies have used a wide range of microparticle sizes from 1 μm to 150 μm, the largest being enough for

human studies [14, 18, 19]. Given that the size of embolic agents is crucially associated with their embolic effect, the huge size discrepancy across animal experiments limits proper interpretation and comparison of the study results. Moreover, evidence concerning treatment effects may be less convincing when microspheres are too large to penetrate the target tissue. Conversely, clinically translating the results of rat embolization experiments conducted using tiny particulates that can wash out to the vein may be unreliable. Thus, to optimize future translational research, the present study aimed to determine the ideal range of sizes for embolic agents in interventional oncology experiments utilizing rat models of HCC.

Materials and Methods

Tumor cell line and Animal model

The McA-RH7777 cell line (CRL-1601; ATCC, Manassas, VA, USA) was cultured in Dulbecco's modified Eagle's medium (DMEM; WelGENE, Daegu, Korea) with 10% fetal bovine serum (WelGENE) and a 1% penicillin–streptomycin mixture (Gibco, Grand Island, NY, USA). To enhance tumor vascularity via overexpression of vascular endothelial growth factor (VEGF), rVEGF-A cDNA (GenBank accession no. NM_031836) was amplified and cloned into a pLenti-Gill lentiviral vector (Applied Biological Materials, Richmond, British Columbia, Canada) [20]. Then, McA-RH7777 cell lines were transfected with the lentivirus to obtain an VEGF-McA-RH7777 cell line. The VEGF-McA-RH7777 cells were maintained in RPMI-1640, and 5×10^6 cells were injected into each rat liver after laparotomy to model rat HCC. To prevent spontaneous tumor regression, cyclosporine A (20 mg/kg/day) was administered subcutaneously from 1 day before tumor implantation until 2 days after surgery.

Study design

he appropriate Institutional Animal Care and Use Committee approved this study, which was performed in accordance with institutional guidelines. Fifty-four male Sprague–Dawley rats were randomly divided into two groups to evaluate the distribution of microparticles in the organs (hereafter,

"distribution group", 39 rats) and to review tumor response by calculating the tumor necrosis rate (hereafter, "tumor response group", 15 rats) (Fig. 1).

Figure 1. Flowchart of the animal model.

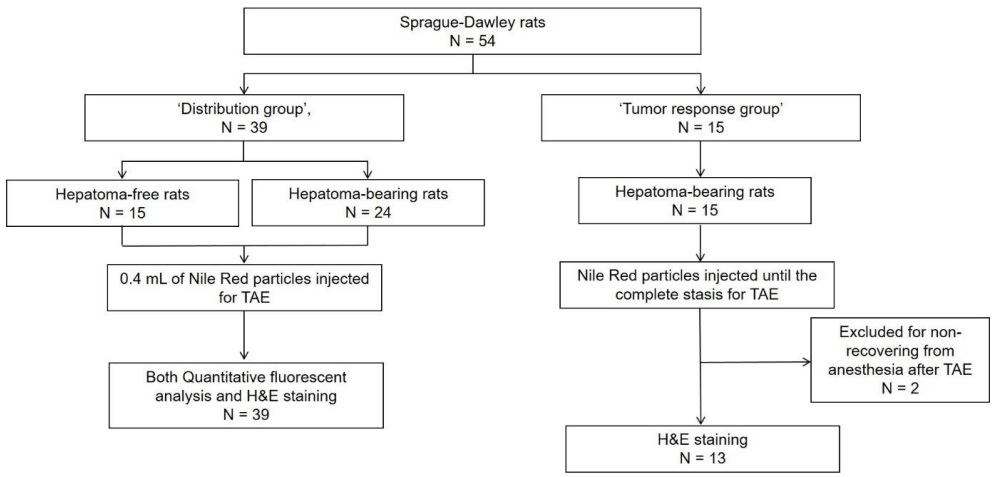

The distribution group was divided into two subgroups: subgroup 1 without hepatoma (15 rats) and subgroup 2, which was inoculated with intrahepatic tumor cells (24 rats). All rats in the tumor response group were implanted with tumor cells. Rats in subgroup 1 underwent transarterial embolization (TAE) of the non-cancerous liver with one of five size ranges of microparticles (5.0–7.9 μm, 10–14 μm, 15–19 μm, 18–24.9 μm, and 25–35 μm). Rats in subgroup 2 and the tumor response group also underwent TAE with microparticles 2 weeks after inoculation of tumor cells, and the tumor growth rate was determined using magnetic resonance imaging (MRI). The embolic endpoint for rats in the distribution group was injection of 0.4 mL of a mixture containing fluorescent microparticles and water. Afterwards,

the distribution of microparticles was evaluated in hepatoma-free rats (subgroup 1), while both the distribution of microparticles and tumor necrosis rate were evaluated in tumor-bearing rats (subgroup 2). The three size ranges of microparticles leading to better tumor response rates than the others in subgroup 2 were chosen for the analysis of tumor necrosis rate in the tumor response group. The embolic endpoint for rats in the tumor response group was injection of microparticles until complete stasis had been achieved on X-ray fluoroscopy.

MRI

MRI was performed using a 3.0-Tesla clinical MRI unit (TrioTim; Siemens Medical Solutions, Erlangen, Germany) with a six-channel rat body coil (Stark Contrast, Erlangen, Germany). Axial T2-weighted turbo spin echo images (TR/TE, 4,180/77ms; flip angle, 140˚; slice thickness, 2 mm; field of view, 80 x 65 mm; matrix, 256 x 177), coronal T2-weighted turbo spin echo images (TR/TE, 6,960/77 ms; flip angle, 140˚; slice thickness, 2 mm; field of view, 84 x 100 mm; matrix, 256 x 184), and axial diffusion-weighted images with single-shot echo planar imaging (TR/TE, 2,100/85 ms; slice thickness, 4 mm; field of view, 80 x 64 mm; matrix, 84 x 68; b-value = 800 s/mm^2) were obtained to identify tumor induction.

Microparticle preparation and Transarterial embolization

Rat TAE was conducted using various sizes of Nile Red particles (SPHERO^{TM} Fluorescent Particles; Spherotech, Inc., Lake Forest, IL). The fluorescent microparticles were prepared by staining polystyrene particles with a fluorophore solution. The fluorophores chosen for use in the preparation of fluorescent particles are water insoluble, and their color and fluorescence remain stable for long periods of time. Nile Red particles are also available in single or multiple fluorophores of various sizes and fluorescence intensities with very small coefficients of variation in both size and fluorescence (Fig 2.).

Figure 2. Size distribution of Nile Red particles (15-19 μm).

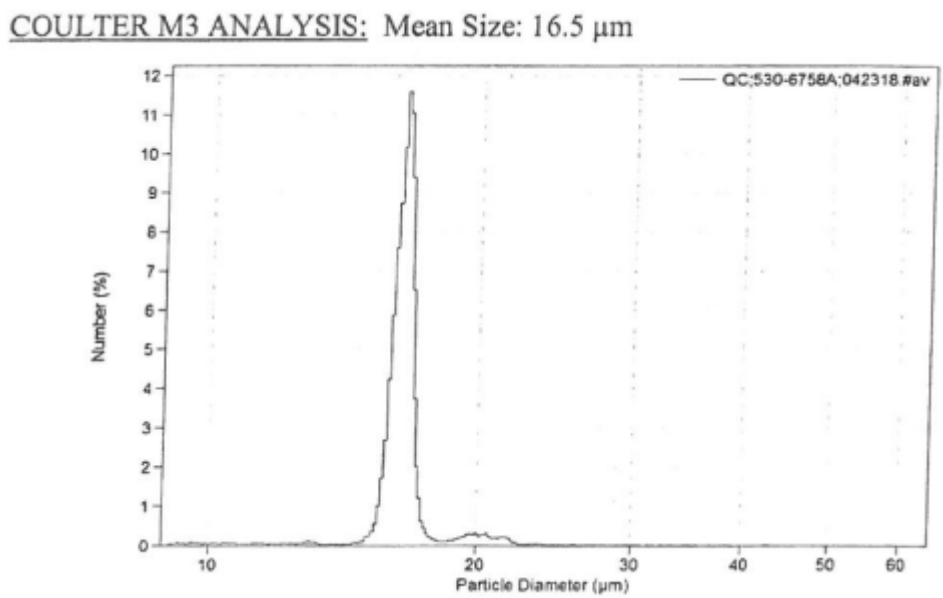

The total volume of Nile Red particles per unit was 2-5 mL with 1% weight/volume ratio. Nile Red particles within the ranges of 5.0–7.9 μm, 10–14 μm, 15–19 μm, 18–24.9 μm, and 25–35 μm were used for analysis in

the distribution group. TAE was performed by one experienced interventional radiologist with 10 years of experience in translational research using an angiography machine. Under anesthesia using zolazepam (5 mg/kg, Zoletil; Virbac, Carros, France) and xylazine (10 mg/kg, Rompun; Bayer Schering, Berlin, Germany), the left common carotid artery was approached after dissecting the neck muscles. A 1.7-Fr microcatheter (Progreat lambda; Terumo Medical Corporation, Tokyo, Japan) was advanced into the proper hepatic artery under the guidance of fluoroscopic imaging. TAE was performed in both the distribution and tumor response groups at the level of the common hepatic artery using the microcatheter.

Quantitative fluorescent and Histologic analyses

All rats were euthanized in a CO_2 chamber 1 week after the procedure. For subsequent quantitative fluorescent and histological analyses, axial sections were obtained across the center of the tumor (in cases of tumor-bearing rats), normal liver, lung, and kidney. The halves of each section were frozen in liquid nitrogen for subsequent quantitative fluorescent analysis. One slice of frozen section (thickness, 4 μm) was obtained for each organ and tumor. Then, the numbers of microparticles in the organs and tumor were measured using a fluorescent microscope under 100X magnification by one investigator (S.H.K) blinded to the treatment allocation. The investigator selected three hot spots (700 x 520 μm per spot) per tissue for counting the number of microparticles, and the mean value

from the three hot spots was recorded to evaluation the microparticle distribution. The remaining halves of each section were fixed in 10% buffered formaldehyde solution and were paraffin embedded. Hematoxylin & eosin (H&E) staining was performed for each section. The tumor necrosis rate was calculated by dividing the area of non-viable portions of the tumor by the total area of the tumor based on digitalized H&E images (Fig. 3).

Figure 3. Transarterial embolization with 18–24.9 μm Nile Red particles in a representative rat model of hepatoma.

(A) Coronal T2-weighted MRI showing a round tumor (arrow) in the liver.

(B) A fluoroscopic image during the injection of microparticles showing stagnation of the iodinated contrast medium in the tumor (arrow).

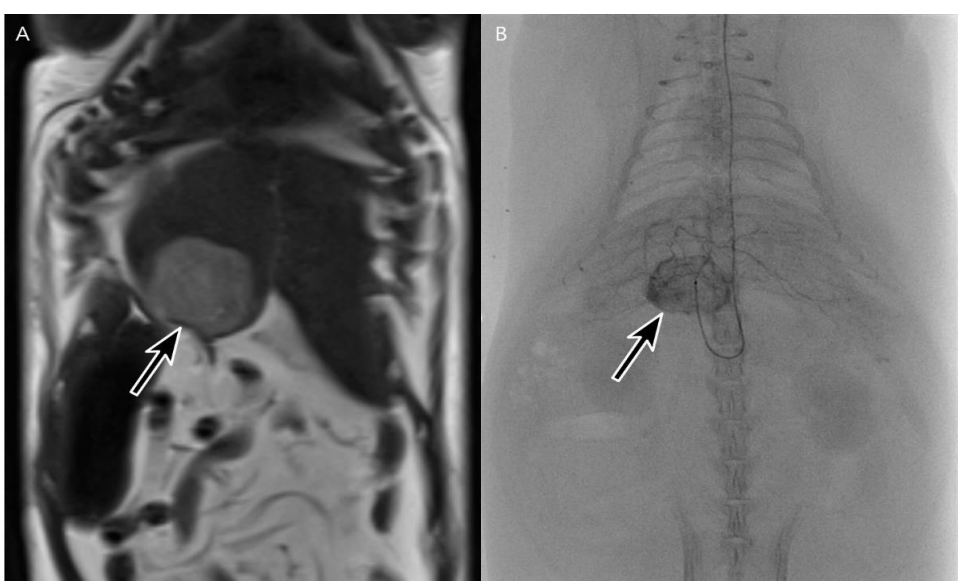

(C) The tumor was harvested after the procedure and frozen-sectioned.

(D) Hematoxylin-and-eosin-stained tissue showing near-complete necrosis of the tumor.

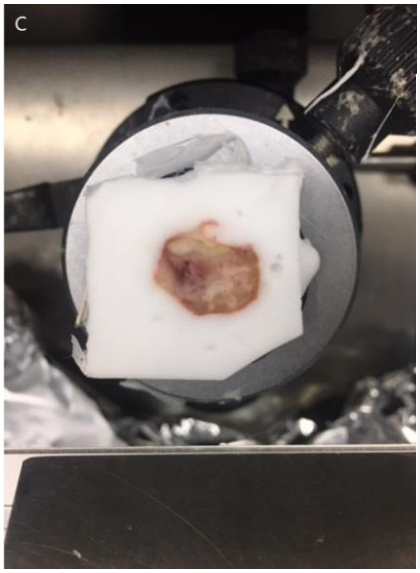

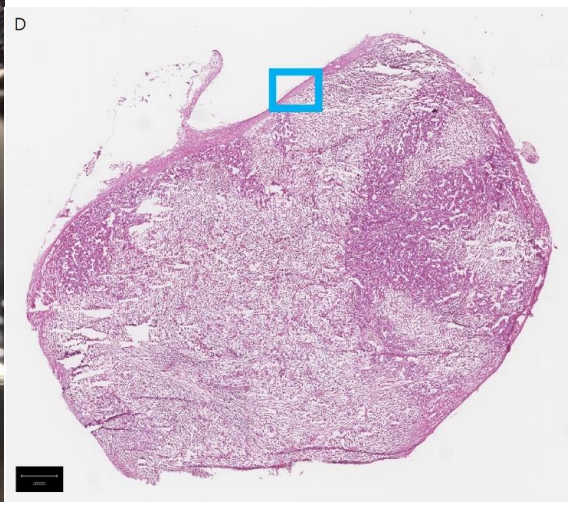

(E) Fluorescence microscopy showing nine microparticles in a single hotspot (blue box in D) from the tumor.

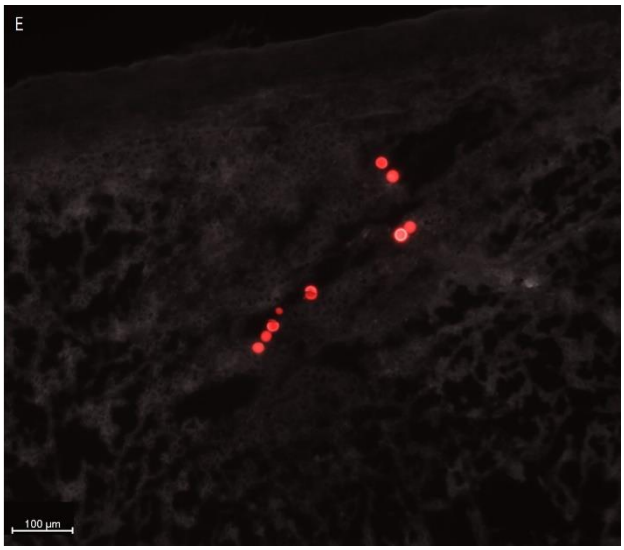

The injury to the normal liver parenchyma was evaluated in all rats of tumor response group using digitalized H&E images.

Statistical analysis

Median values for each size range were used to compare microparticle distributions in each organ and tumor. The Kruskall–Wallis test was used to compare the tumor necrosis rate among the three different microparticle sizes in the tumor response group. A two-sided p-value < 0.05 was considered statistically significant. The statistical analysis was performed using commercial statistics software (MedCalc, version 19.2; MedCalc, Ostend, Belgium).

Results

Distribution of microparticles in hepatoma-free rats

There was a non-target organ distribution tendency, as the microparticle size became smaller. Microparticles were detected in the lung in all rats using the size of 5.0-7.9 μm of Nile Red particles, whereas those were detected in the lung in one out of three rats when sizes of 10-14 μm, 15-19 μm, and 18-24.9 μm Nile Red particles were used for TAE. None of microparticles was detected in the lung when 25-35 μm sized Nile Red particles was used for TAE. No microparticles were detected in the kidney except for only one rat using the size of 5.0-7.9 μm of Nile Red particles for TAE (Table 1). The liver was the organ where the largest number of microspheres were found, irrespective of the sizes.

Table 1. The number of microparticle counts distributed in each organ of hepatoma-free rats.

Rat number	**Particle size (μm)**	**Liver**	**Lung**	**Kidney**
#1	5.0 - 7.9	24	5	1
#2	5.0 - 7.9	26	5	0
#3	5.0 - 7.9	18	2	0
#4	10 - 14	9	1	0
#5	10 - 14	4	0	0
#6	10 - 14	6	0	0
#7	15 - 19	6	0	0
#8	15 - 19	3	1	0

#9	15 - 19	6	0	0
#10	18 - 24.9	7	1	0
#11	18 - 24.9	6	0	0
#12	18 - 24.9	13	0	0
#13	25 - 35	16	0	0
#14	25 - 35	18	0	0
#15	25 - 35	11	0	0

Distribution of microparticles in tumor-bearing rats

A similar tendency for non-target organ distribution was observed in tumor-bearing rats when compared with hepatoma-free rats. Nile Red particles of 5.0–7.9 μm in size were more frequently observed in the normal liver parenchyma and lung than those of larger sizes (Fig. 4).

Figure 4. A bar graph showing the median numbers of microparticles in the tumor and organs according to microparticle size.

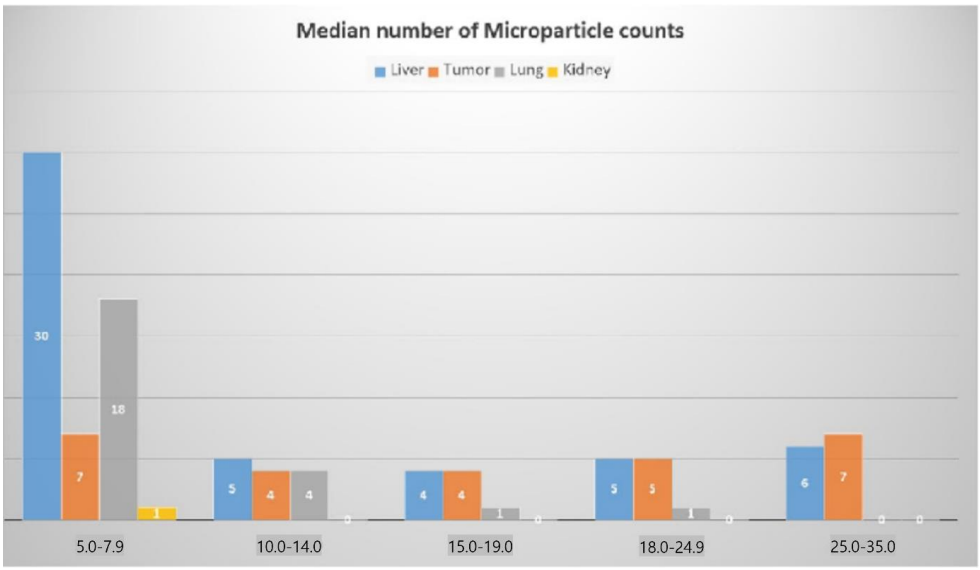

When Nile Red particles were larger than 15 μm in size, only a few microparticles (≤ 3) were detected in the lung, except in one rat. Of note, fifteen microparticles were detected in the lung in one rat injected with 18–24.9-μm Nile Red particles, probably due to large shunt development associated with the tumor. The microparticle counts in the tumor and each organ are listed in Table 2.

Table 2. The number of microparticle counts distributed in the tumor and each organ of tumor-bearing rats.

Rat number	**Particle size (μm)**	**Liver**	**Tumor**	**Lung**	**Kidney**	**Tumor necrosis rate (%)**	**Mean tumor necrosis rate (%)**
#1	5.0 - 7.9	13	3	36	4	10	
#2	5.0 - 7.9	23	1	9	0	5	
#3	5.0 - 7.9	48	11	7	2	15	10
#4	5.0 - 7.9	37	11	27	0	10	
#5	10 - 14	4	2	2	0	95	
#6	10 - 14	5	1	1	0	90	
#7	10 - 14	5	4	4	0	25	50
#8	10 - 14	12	9	5	0	30	
#9	10 - 14	15	5	4	0	10	
#10	15 - 19	2	5	0	0	90	
#11	15 - 19	4	7	1	0	90	
#12	15 - 19	3	2	3	0	15	71
#13	15 - 19	6	2	0	0	90	
#14	15 - 19	7	4	1	0	70	

#15	18 - 24.9	2	5	1	0	95	
#16	18 - 24.9	6	16	1	0	95	85
#17	18 - 24.9	13	15	1	0	90	
#18	18 - 24.9	5	5	0	0	95	
#19	18 - 24.9	4	5	15	0	50	
#20	25 - 35	8	17	0	0	40	
#21	25 - 35	2	2	1	0	100	
#22	25 - 35	3	15	1	0	95	80
#23	25 - 35	8	5	0	0	85	
#24	25 - 35	6	7	0	0	80	

Tumor response according to microparticle size

When TAE was performed using a pre-determined amount (0.4 mL) of microparticles (subgroup 2 in distribution group), rates of necrosis were highest in rats injected with particle sizes of 15–19 μm (mean necrosis rate, 71%), 18–24.9 μm (85%), and 25–35 μm (80%). Therefore, these size ranges were re-evaluated in the tumor response group. Among the fifteen rats (five for each size range), one rat in the 15–19 μm group and one rat in the 18–24.9 μm group died after anesthesia for TAE and were thus excluded from the analysis. Therefore, a total of 13 rats were euthanized for analysis after performing TAE with an embolic endpoint of complete stasis. The

amount of microparticles used in rats of the tumor response group ranged from 0.8 mL to 1.5 mL. As a result, tumor necrosis rates tended to be higher in rats treated with 15–19-μm Nile Red particles (mean, 99%) than in those treated with particle sizes of 18–24.9 μm (75.3%) or 25–35 μm (57.8%) (Table 3).

Table 3. Tumor necrosis rate in dependency of microparticle size.

Rat number	**Particle size (μm)**	**Tumor necrosis rate (%)**	**Mean of tumor necrosis rate (%)**
#1	15-19	100	99.0
#2	15-19	100	
#3	15-19	100	
#4	15-19	96	
#5	18-24.9	42	75.3
#6	18-24.9	100	
#7	18-24.9	85	
#8	18-24.9	74	
#9	25-35	57	57.8
#10	25-35	100	
#11	25-35	34	
#12	25-35	76	
#13	25-35	22	

Injury to the normal liver parenchyma was not observed in all rats of tumor response group (Fig. 5).

Figure 5. Transarterial embolization with 15–19 μm Nile Red particles.

(A) The tumor and adjacent normal liver parenchyma were harvested after the procedure and frozen-sectioned.

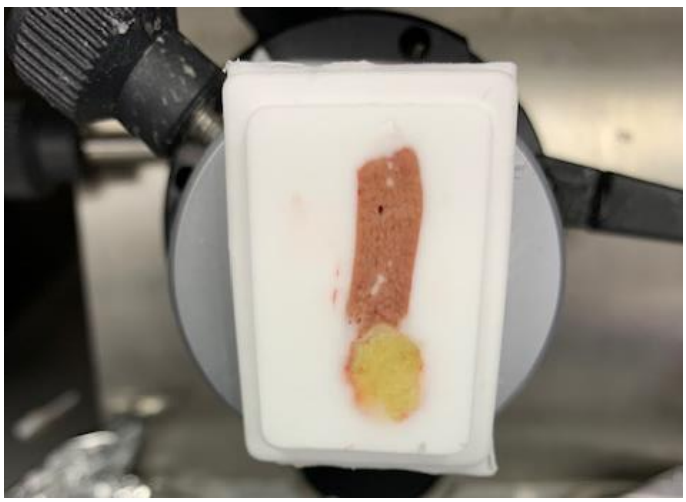

(B, C) Hematoxylin-and-eosin-stained tissue showing near-complete necrosis of the tumor and no injury to the adjacent liver parenchyma.

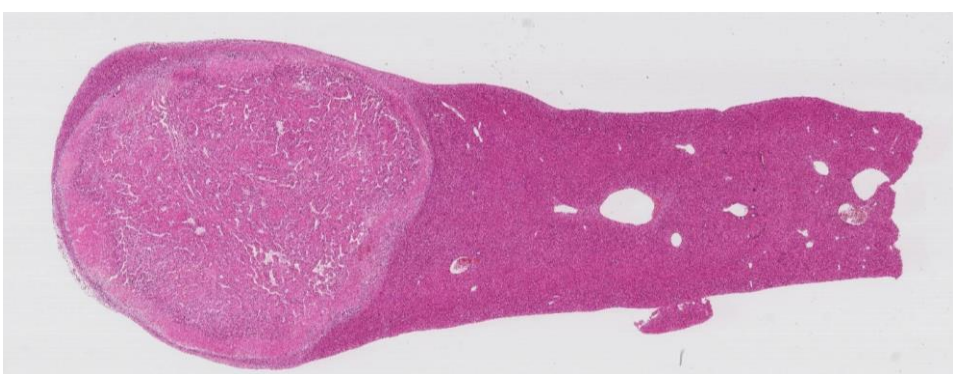

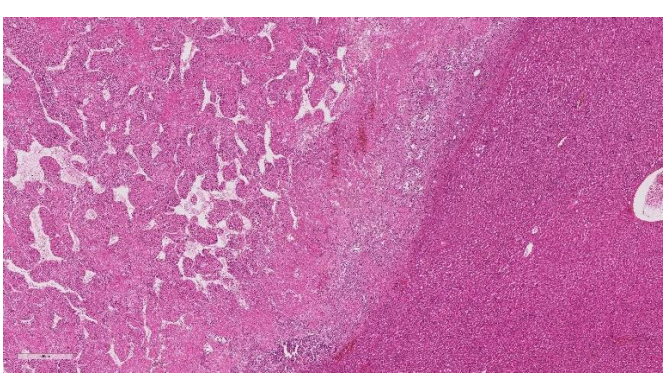

The within-group variability of tumor necrosis rates was high in rats treated with particle sizes of 18–24.9 μm and 25-35 μm, which implies proximal embolization of the hepatic artery when larger microparticles are used. However, there were no statistically significant differences in tumor necrosis rates among the three groups (p = .095) (Fig. 6).

Figure 6. Box plots of the tumor necrosis rate according to different microparticle sizes. Upper, middle, and lower horizontal bars represent the maximum value, median value, and minimum value, respectively. Upper and lower margins of the candle represent the upper and lower quartiles, respectively.

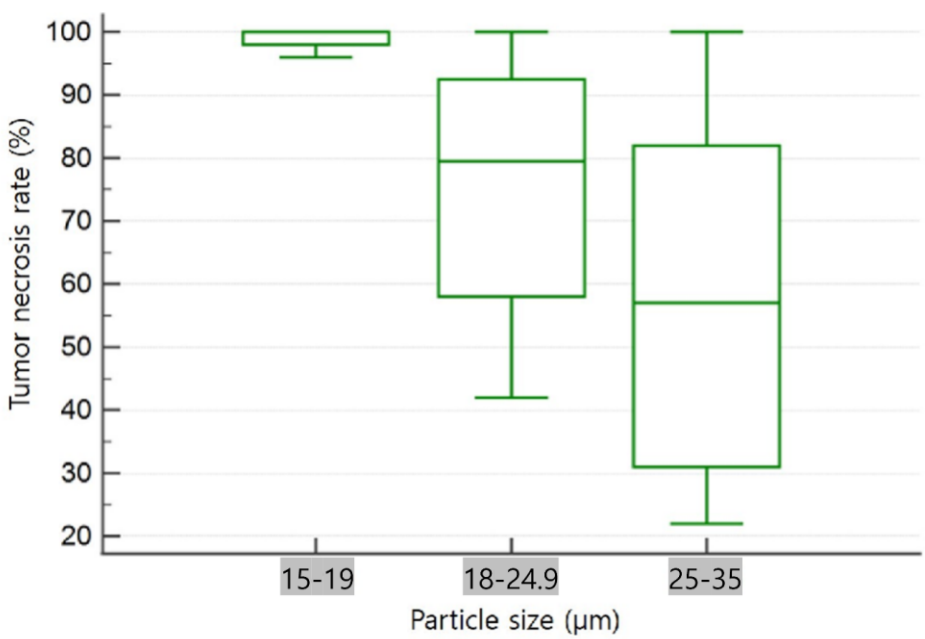

Discussion

Although previous studies using animal models of HCC have focused on the embolic effect following TAE, their results remain controversial [14, 18, 19]. Our findings suggest that the ideal size range for embolic agents in rat models of HCC is 15-19 μm. Furthermore, a size larger than 15 μm is recommended for preventing undesirable distribution to the lung in such models.

The size of embolic agents in animal experiments should be carefully determined to achieve reliable results mirroring human practice. Microspheres that are too small can be harmful to the patient. A previous study reported that the diameters of terminal arterioles and capillaries in rats are 10–50 μm and 8–10 μm, respectively [21]. This may explain the tendency for microparticle distribution in the lung in hepatoma-free rats in the 5.0–7.9-μm group, as this is smaller than the capillary diameter in rats. In contrast, when microparticles ≥ 10 μm in size were used for TAE in hepatoma-free rats, most microparticles were detected in the liver parenchyma. Conversely, microparticles that are too large will not induce sufficient embolic effects. A pre-clinical study using a rabbit tumor model failed to obtain tumoricidal effects using large embolic agents (≥ 70 μm), even when complete stasis was achieved during TAE [22]. In accordance

with previous results, our findings indicate that the rate of tumor response dependeds on the size of microparticles used for TAE.

Bastian et al. [23] reported that an embolic agent with a mean diameter of 40 μm is required for hepatic artery embolization without shunting to other organs considering the size of hepatic artery in rats. These results are in contrast to those of our study, which indicated that a size of 15–19 μm yielded the best tumor necrosis rate when compared with larger sizes. However, the embolic materials used in the previous study were prepared using a modified solvent evaporation method, which inevitably produces a wide range of particle sizes: For example, the size range for the embolic agents with a mean diameter of 40 μm in the previous study extended from approximately 1 to 100 μm [23]. Conversely, the microparticles used in the present study had a very small coefficient of variation in size (e.g., 4 to 10 μm), suggesting that the current findings are more reliable. Considering the present results, embolic agents in the range of 15–19 μm are sufficient for obtaining tumoricidal effects in rat hepatoma models, whereas microparticles larger than 15–19 μm may be less effective in this regard due to proximal embolization of the hepatic artery, which results in less hypoxic damage to the hepatoma.

In this study, we observed a difference in the distribution of microparticles to the lung between hepatoma-bearing rats and hepatoma-free rats. As mentioned above, microparticles larger than 10 μm were hardly distributed to the lung in hepatoma-free rats. However, 10–14-μm

microparticles were well distributed to the lung in hepatoma-bearing rats even though their diameter was larger than that of rat capillaries. Such results can be explained by arteriovenous shunting, which is frequently observed in cases of hypervascular tumors such as HCC [24, 25]. In addition, we observed that median values of distribution of microparticles to the tumor and normal liver parenchyma are similar. Such findings are possibly because vascularity of rat hepatoma is less prominent than that observed in human HCC. Another explanation for such findings is probably that we used predetermined amount of embolic agents for distribution analysis.

This study had several limitations. First, the sample size in each size group was small given the various size ranges examined, making it difficult to identify statistically significant effects among the groups. Second, tumors in rat hepatoma models have relatively homogenous features, and their vascularity is less prominent than that observed in human HCC. Finally, detection error may have occurred in counting the number of microparticles in each organ and tumor. Microparticles counts were recorded as the mean value for only three hot spots per tissue, which is less accurate than counting microparticles in the whole tissue. However, the same method was used for all microparticle sizes in each organ and the tumor, which may have reduced the likelihood of sampling error. Despite these limitations, the present results suggest that embolic agents ranging in size from 15–19 μm should be considered as the first option for achieving tumoricidal effects via

transarterial treatments in rat models of HCC.

Bibliography

[1] Cho HR, Choi JW, Kim H-C, et al. Sprague-Dawley rats bearing McA-RH7777 cells for study of hepatoma and transarterial chemoembolization. Anticancer research 2013; 33:223-30.

[2] Lee K-H, Liapi EA, Cornell C, et al. Doxorubicin-loaded QuadraSphere microspheres: plasma pharmacokinetics and intratumoral drug concentration in an animal model of liver cancer. Cardiovascular and interventional radiology 2010; 33:576-82.

[3] Sheu AY, Zhang Z, Omary RA, Larson AC. MRI-monitored transcatheter intraarterial delivery of SPIO-labeled natural killer cells to hepatocellular carcinoma: preclinical studies in a rodent model. Investigative radiology 2013; 48:492.

[4] Gordon AC, Lewandowski RJ, Salem R, Day DE, Omary RA, Larson AC. Localized hyperthermia with iron oxide–doped yttrium microparticles: Steps toward image-guided thermoradiotherapy in liver cancer. Journal of Vascular and Interventional Radiology 2014; 25:397-404.

[5] Wu L, Tang Z-Y, Li Y. Experimental models of hepatocellular carcinoma: developments and evolution. Journal of cancer research and clinical oncology 2009; 135:969-81.

[6] Zhang Y, White SB, Nicolai JR, et al. Multimodality imaging to assess immediate response to irreversible electroporation in a rat liver tumor model. Radiology 2014; 271:721-9.

[7] Choi JW, Kim H, Kim H-C, et al. Blood oxygen level-dependent MRI for evaluation of early response of liver tumors to chemoembolization: an animal study. Anticancer research 2013; 33:1887-92.

[8] Li X, Wang Y-XJ, Zhou X, Guan Y, Tang C. Catheterization of the hepatic artery via the left common carotid artery in rats. Cardiovascular and interventional radiology 2006; 29:1073-6.

[9] Jiang H, Meng Q, Tan H, et al. Antiangiogenic therapy enhances the efficacy of transcatheter arterial embolization for hepatocellular carcinomas. International journal of cancer 2007; 121:416-24.

[10] Hanada M, Baba A, Tsutsumishita Y, et al. Intra-hepatic arterial administration with miriplatin suspended in an oily lymphographic agent inhibits the growth of tumors implanted in rat livers by inducing platinum-DNA adducts to form and massive apoptosis. Cancer chemotherapy and pharmacology 2009; 64:473-83.

[11] Garin E, Denizot B, Roux J, et al. Description and technical pitfalls of a hepatoma model and of intra-arterial injection of radiolabelled lipiodol in the rat. Laboratory animals 2005; 39:314-20.

[12] Ju S, McLennan G, Bennett SL, et al. Technical aspects of imaging and transfemoral arterial treatment of N1-S1 tumors in rats: an appropriate model to test the biology and therapeutic response to transarterial treatments of liver cancers. Journal of Vascular and Interventional Radiology 2009; 20:410-4.

[13] Thompson SM, Callstrom MR, Knudsen B, et al. Development and

preliminary testing of a translational model of hepatocellular carcinoma for MR imaging and interventional oncologic investigations. Journal of Vascular and Interventional Radiology 2012; 23:385-95.
[14] Chen J, Sheu AY, Li W, et al. Poly (lactide-co-glycolide) microspheres for MRI-monitored transcatheter delivery of sorafenib to liver tumors. Journal of Controlled Release 2014; 184:10-7.
[15] Wang G-Z, Fang Z-T, Zhang W, et al. Increased metastatic potential of residual carcinoma after transarterial embolization in rat with McA-RH7777 hepatoma. Oncology reports 2014; 31:95-102.
[16] Choi JW, Kim JH, Kim H-C, et al. Comparison of tumor vascularity and hemodynamics in three rat hepatoma models. Abdominal Radiology 2016; 41:257-64.
[17] Choi JW, Kim H-C, Baek SY, Ryu YJ, Chung JW. A metastatic hepatoma model of rats using the 13762-MAT-B-III cell line: basic characteristics and potential as a tool for interventional oncology experiments. Anticancer research 2015; 35:1333-8.
[18] Cortes AC, Nishiofuku H, Polak U, et al. Effect of bead size and doxorubicin loading on tumor cellular injury after transarterial embolization and chemoembolization in a rat model of hepatocellular carcinoma. Nanomedicine: Nanotechnology, Biology and Medicine 2022; 39:102465.
[19] Minamiguchi K, Tanaka T, Nishiofuku H, et al. Comparison of embolic effect between water-in-oil emulsion and microspheres in transarterial embolization for rat hepatocellular carcinoma model. Hepatology Research

2020; 50:1297-305.

[20] Choi JW, Cho HR, Lee K, Jung JK, Kim H-C. Modified rat hepatocellular carcinoma models overexpressing vascular endothelial growth factor. Journal of Vascular and Interventional Radiology 2018; 29:1604-12.

[21] Burkel WE. The fine structure of the terminal branches of the hepatic arterial system of the rat. The Anatomical Record 1970; 167:329-49.

[22] Levy EB, Johnson CG, Jacobs G, et al. Direct quantification and comparison of intratumoral hypoxia following transcatheter arterial embolization of VX2 liver tumors with different diameter microspheres. Journal of Vascular and Interventional Radiology 2015; 26:1567-73.

[23] Bastian P, Bartkowski R, Köhler H, Kissel T. Chemo-embolization of experimental liver metastases. Part I: distribution of biodegradable microspheres of different sizes in an animal model for the locoregional therapy. European journal of pharmaceutics and biopharmaceutics 1998; 46:243-54.

[24] Itai Y, Furui S, Ohtomo K, et al. Dynamic CT features of arterioportal shunts in hepatocellular carcinoma. American journal of roentgenology 1986; 146:723-7.

[25] Choi BI, Lee KH, Han JK, Lee JM. Hepatic arterioportal shunts: dynamic CT and MR features. Korean Journal of Radiology 2002; 3:1-15.